Proceedings of the 1st Global Power and Propulsion Forum
GPPF 2017
Jan 16-18, 2017, Zurich, Switzerland
www.pps.global

GPPF-2017-175

MEASURING THE IMPACT OF JACKING-OIL PORTS ON THE ROTORDYNAMIC CHARACTERISTICS OF A FOUR-PAD, LBP, TILTING-PAD JOURNAL BEARING

Matthew Kluitenberg
Turbomachinery Laboratory
Texas A&M University
mpkluity@gmail.com
College Station, TX

Dara Childs
Turbomachinery Laboratory
Texas A&M University
dchilds@tamu.edu
College Station, TX

ABSTRACT

This paper examines the influence of inactive jacking-oil ports on a tilting pad journal (TPJ) bearing by comparing measured static and dynamic test results of the bearing with and without ports. The TPJ is a four-pad, rocker-pivot, 57% pivot offset in the load-between-pad (LBP) configuration. It was originally tested by Tschoepe and Childs, and later modified to include a jacking-oil recess on each loaded pad, and retested with the same test rig, procedure, and operating conditions. Tests only considered the no-pressurized ports. Measured static characteristics include the static-load equilibrium eccentricity and attitude angle, bearing clearance, and pad metal temperatures. The rotordynamic characteristics are presented as dimensionless coefficients, following a frequency-independent [K][C][M] model.

Adding jacking-oil ports causes a decrease in direct damping by an average of 26% in the loaded direction, and 9% in the orthogonal direction. They also caused an increase in direct virtual-mass (from negative towards positive), from all negative, to a mixture of positive and negative that are smaller in magnitude. No significant changes were observed in any of the cross-coupled coefficients or the direct stiffness coefficients. Additionally, there were no noticeable changes in the static performance of this TPJ bearing. Efforts made to model the bearing with the added recesses were generally unsuccessful. Rotordynamic predictions are presented for a simple Rigid-rotor/bearing system, using measured dynamic coefficients that show adding jacking-oil ports can: (1) significantly lower the first critical speed, and (2) reduce the damping ratio at the critical speed.

The measured results and rigid-rotor model predictions suggest that implementing JO ports in a machine supported by tilting pad bearings will cause a drop in the observed 1st critical speed and an increase in its associated damping factor.

INTRODUCTION

The work reported here was generated by a request from an engineer from a large OEM based on his company's experience on machines that used jacking-oil (JO) ports with tilting-pad journal bearings (TPJBs). They had generally good outcomes in predicting rotor response for rotors supported by TPJBs without JO ports. However, the outcomes for predicting the response after adding JO ports (but using the same bearing codes) was considerably less accurate. Based on that field experience, the engineer wanted tests to compare the static and rotordynamic performance of a TPJB with and without JO ports.

JO ports are added to the bearing to eliminate rubbing at low speeds. Pressurized oil is injected into ports (recesses or pockets) on the pad surface. The jacking-oil is only used at start up and shut down and is not used at full-speed operation. This solution is most common in fixed-arc bearings. However, some recent applications include TPJ bearings. The impact of adding jacking-oil ports on rotordynamics for TPJs is unknown.

A limited amount of work relating to TPJ bearings with jacking-oil exists. Santos and Russo [2] provide both theoretical and experimental studies of a TPJ with "electronic radial oil injection [2]." Varella and Santos [3] use active lubrication to change the bearing's stiffness and damping coefficients by controlling the pressure of the injection oil.

The 2009 case study by Hattenbach and Sandberg [4] investigated the source of super-synchronous vibrations in a motor that used jacking-oil. The original four-lobe fixed-geometry bearings were replaced with a four-pad TPJ bearings (with jacking-oil) to eliminate a vibration problem. Further testing revealed that the volume of oil trapped in the

supply lines caused the super-synchronous vibrations. A new design including a check valve within the bearing housing, limiting the volume of oil, eliminated the problem. Hagemann et al. **Error! Reference source not found.** compared measured and predicted static data for a large TPJ bearing with jacking-oil.

In 2013, Ressing et al. [6] presented a case study regarding subsynchronous vibrations in an axial gas compressor operating on two-lobe bearings with two JO ports in the lower (loaded) pads. Check valves were provided to prevent back flow. The two ports in a bearing were connected to a bypass line (well) outside the bearing. Subsynchronous vibrations that were observed with the bypass valve closed dropped by 70% when the valve was opened. Measured bearing test results for the bearing were reported from a test rig at the Canadian research Center in Ottawa.

No published work provides a comparison of a TPJ bearing with and without inactive (no external pressure) jacking-oil ports. The present work determines the effects of inactive jacking-oil recesses by comparing measured static and rotordynamic characteristics of a TPJ bearing with and without jacking ports. The TPJ bearing is a four-pad, rocker-pivot, in load-between-pad (LBP) configuration. Tschoepe and Childs [1] reported test results for the original bearing (no jacking-oil ports) in 2011, and their data provides the basis for comparison

DESCRIPTION OF THE TEST RIG

Test Apparatus

The bearing test rig is based on the floating-bearing design, introduced by Glienicke [7] in 1967, in which the test bearing is free to move about a rigidly-supported shaft. Figure 1 shows a section view of this rig.

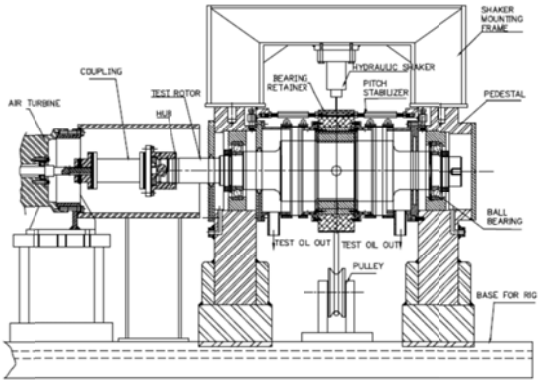

Figure 1. Test rig cross-section view, figure from [8]

The main test section consists of a bearing assembly, supporting pedestals, static loader, two dynamic loaders, and a rotor driven by an air turbine. The rotor is supported by angular-contact ball bearings on two pedestals that are preloaded to ensure contact between the balls and bearing race.

The "stator assembly" consists of the test bearing, bearing end-seals, end-caps, and a steel housing referred to as the stator. The stator connects the bearing to the pitch stabilizers, oil supply, static loader, two hydraulic shakers, and various instrumentation. The pitch stabilizers prevent pitching and yawing of the stator during excitation. Aluminium end-caps are attached on either side of the stator.

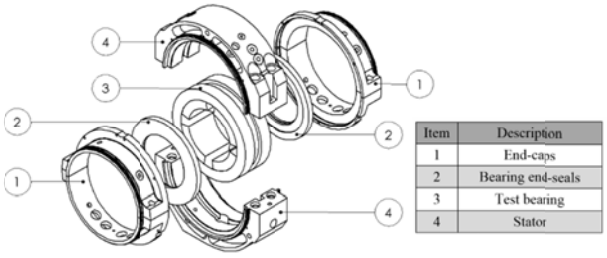

Item	Description
1	End-caps
2	Bearing end-seals
3	Test bearing
4	Stator

Figure 2. Exploded view of test bearing assembly

This bearing uses flooded lubrication. Oil enters through four holes in the bearing housing and exits through the bearing end-seals, which restrict the flow.

Bearing load is applied to the stator via a pneumatic actuator. The actuator is connected to the stator housing through a spring, steel cable, and pulley wheel. This assembly allows for small movement of the stator while maintaining a constant load direction and magnitude. The stator is pulled in the +*y*-direction simulating a rotor load in the -*y*-direction.

Two hydraulic shakers apply dynamic loads to the stator. The shakers are mounted in orthogonal directions with one shaker in-line with the static loading direction. Each shaker head is connected to the stator through a load cell and a stinger. The shaker static forces are adjusted before testing until the weight of they support the bearing assembly weight, and the bearing is centered about the rotor.

Instrumentation

The rotor speed, static load, oil flow rate, and inlet oil temperature are controlled. Figure 3 shows the stator assembly with instrumentation and additional hardware including stingers, pitch stabilizers (end view), static load connection, and the inlet oil connection. The bearing end-seal is removed to show the pads (shaded) and load orientation.

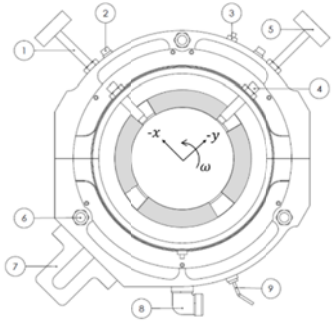

Item	Description	Quantity
1	Stinger	2
2	Accelerometer	2
3	Pressure transducer	3
4	Proximity probe	4
5	Load cell	2
6	Pitch stabilizer	6
7	Static load connection	1
8	Oil inlet connection	1
9	Oil inlet thermocouple	1

Figure 3. DE view of stator assembly with instrumentation, figure adapted from [9]

Proximity probes (eddy current sensors) measure the relative displacement between the rotor and bearing. A set of probes is mounted in the stator end-cap on both the drive end (DE) and non-drive end (NDE) of the bearing. Each set has one proximity probe mounted in the *x*-direction and another in the *y*-direction. Two piezoelectric accelerometers measure the absolute acceleration of the bearing in both the *x* and *y* directions. Load cells attached between the hydraulic shakers and the stingers measure the force applied by each shaker during dynamic tests.

The test bearing contained twenty-one type-K thermocouples embedded in the pads to measure the thermal

gradients across the loaded pads, and estimate the thermal deflection in the pads. Space constraints preclude presentation of the temperature data in this paper.

Bearing Description

Table 1 lists the nominal properties of the test bearing.

Table 1. Nominal bearing properties

Property	Values
Bearing type	Four-pad, rocker-pivot
Configuration	LBP
Pivot offset	57%
Preload	0.3
Pad arc angle	72°
Rotor diameter	101.524 mm (3.997 in)
Bearing (bore) diameter	101.758 mm (4.0062 in)
Radial pad clearance	0.118 mm (0.00465 in)
Radial bearing clearance	0.0826 mm (0.00325 in)
Pad axial length	60.33 mm (2.375 in)
Pad mass	0.96 kg

Figure 4 illustrates the recesses. Each recess reduces the surface area of the pad by 5.2%, and the recess depth is 2.11 mm (0.083 in) or 25.5 times the nominal radial bearing clearance. The recesses are located directly above the pad pivots.

JO supply lines were attached to both loaded pads. Prior to testing, oil was pushed through the supply lines were used to purge the jacking recesses of air. Jacking-oil was not used during testing. Each line contains a check valve to ensure that oil does not exit the bearing through the supply lines during testing. In practice, check valves are typically mounted inside the pad pivot, but the rocker pivot pads used here did not allow this method. As shown in Figure 4, check valves were added very close to the pad to minimize the volume of trapped oil.

.

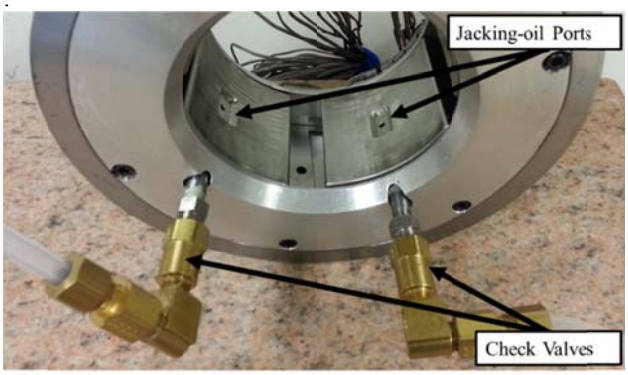

Figure 4. Modified test bearing with attached jacking-oil supply lines

The Babbitt layer on pad #1 was damaged during previous testing and replaced during the modification process. Stainless-steel shims were placed behind pads #1 and #3 to replicate the bearing clearance measured by Tschoepe and Childs.

EXPERIMENTAL PROCEDURE

The modified bearing tests used the same operating conditions and experimental procedure as used in [1], with the exception of the oil temperature and bearing centering method. This section provides the operating conditions, describes the procedures used to measure static and dynamic characteristics, and discusses these two changes.

Operating Conditions

Testing is completed at the same nominal conditions used previously [1]. Each test series includes the four speeds and four load summarized in (Table 2).

Table 2. Nominal testing conditions

Unit load [kPa (psi)]	Speed [RPM], (flow-rate [L/min])			
	6,800 (22.7)	9,000 (26.5)	10,800 (30.3)	13,200 (34.1)
725 (105.3)	X	X	X	X
1,452 (210.5)	X	X	X	X
2,177 (315.8)	X	X	X	□
2,903 (421.1)	X	X	X	□

X = *results for both bearings presented*
□ = *results presented only for modified bearing*

The modified bearing was tested with ISO VG 46 oil and an inlet oil temperature of 54.7°C (130.5°F) for all test points. The original bearing was tested with ISO VG 32 and an inlet temperature of 43.3°C (110°F). The increased inlet oil temperature was selected to get the same oil viscosity for both bearings.

Results from [1] do not include unit loads of 2.177 and 2.903 MPa at 13,200 rpm. The original bearing was tested at incorrect unit loads for these conditions. This discrepancy was only realized after completing the jacking-oil modifications, when the original bearing could not be retested

Static Characteristics

For each point in the test matrix, testing begins by bringing the test rig to thermal steady-state operation as close to the nominal test conditions as possible. Static measurements are made first, followed by dynamic measurements. The data acquisition system records all static conditions 20 times over a span of 40 seconds. Static data for a single test condition are the average of these 20 samples.

The four proximity probes measure the journal position in the x and y directions relative to the bearing center (x_o, y_o). The DE and NDE measurements are averaged to provide a single position measurement located at the bearing center plane. As shown in Figure 5, the rotor position (x_r, y_r) relative to the geometric bearing center (x_o, y_o) can be expressed in terms of eccentricity ratio $\varepsilon_o = e_0 / C$ where e_o is the static displacement and C is the radial clearance. The attitude angle γ is positive in the direction of shaft rotation.

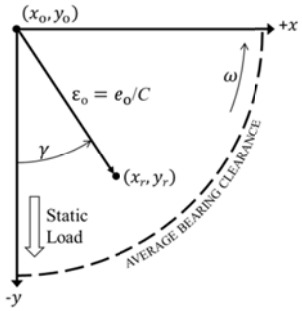

Figure 5. Static displacement coordinate system

Clearance Measurement

To measure the bearing clearance, the hydraulic shakers slowly precess the bearing around the rotor. The applied force is large enough to maintain contact between the pads and rotor creating a "pad profile" as shown in Figure 6. The static displacement exceeds the bearing clearance when the load is directed between the rotatable pads. The rectangular shape of Figure 6 arises because of the four pads.

A "cold clearance" refers to a clearance measurement taken at room temperature before the test rig has been started. "Hot clearance" refers to a clearance taken just after testing (within 20 seconds), while the test rig is at an elevated temperature. Both bearing tests include a single cold clearance and one hot clearance for each running speed, taken after testing the highest load.

Each measured pad profile is fitted with a circle to estimate the average bearing clearance and bearing center. Pad corner points are selected on the largest pad outline. Pad center points are estimated by averaging the two surrounding corner points. The bearing center and average bearing clearance are estimated by fitting a circle to the four pad center points. Figure 6 illustrates this process.

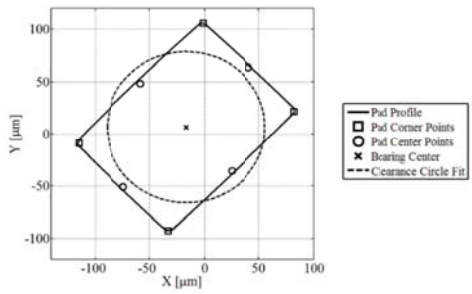

Figure 6. Average clearance fit

The measured hot clearance provides both the bearing center (x_o, y_o) and the average bearing clearance used for calculating eccentricity and nondimensionalizing the dynamic coefficients.

Bearing center

The rotor position relative to the bearing is measured using the two sets of x and y proximity probes located in the stator end-caps. They are averaged to provide a single x and y measurement at the bearing's midplane. The bearing center location is required to determine static displacement, eccentricity, and attitude angle. It is measured while the test rig is at the operational temperature because thermal expansion shifts the bearing center position. The bearing center is different for each running speed.

Some previous work (including [1]) used a zero-load test to determine the bearing center. The present method uses the hot-clearance method discussed by Coghlan and Childs [10].

Dynamic Characteristics

Dynamic measurements are made after completing the static measurements for a given operating condition. The hydraulic shakers excite the stator in the x and y directions separately. The bearing response is recorded in both orthogonal directions during each excitation. These forced excitations consist of an ensemble of sinusoidal waveforms with frequencies varying from 10 to 250 Hz in 10 Hz increments that are slightly offset to avoid shaking at multiples of 60 Hz. The designed waveform is repeated (without stopping) 320 times and that takes 30 seconds to complete for each direction. The data are divided into 10 data sets each containing 32 shakes. Each data set is averaged separately and then reviewed to determine the repeatability of the measurements.

Parameter Identification Model

The parameter identification method outlined by Rouvas and Childs [11] was used. Tschoepe and Childs [1] used the same approach.

Baseline Data

The attached hardware such as the pitch stabilizers, oil hose, and static loader assembly, affect the stiffness, damping, and the total mass of the bearing assembly. Subtracting a "baseline" accounts for these structural properties and isolates measurements for the fluid film properties. A baseline refers to the measured dynamic response while exciting the bearing assembly with no oil in the bearing and no shaft rotation. The same baseline measurement is used to adjust each dynamic test in the test matrix. A static load of 1,112 N (250 lbf) is applied during the baseline measurement ensuring that the effects from the static loader assembly are included. The baseline is also used to estimate the stator mass (M_s) for the force equation. The baseline dynamic-stiffness coefficient values are subtracted before the curve-fit procedure ensuring that only the bearing (fluid-film) properties are estimated.

$$\boldsymbol{H}_{ij} = \boldsymbol{H}_{ij,\mathrm{TEST}} - \boldsymbol{H}_{ij,\mathrm{BASE}} \tag{1}$$

Dimensionless Coefficients

Dynamic coefficients are presented as dimensionless quantities, denoted by lower case constants k_{ij}, c_{ij}, and m_{ij}.

$$k_{ij} = K_{ij}\left(\frac{C_b}{F_s}\right) \tag{2}$$

$$c_{ij} = C_{ij}\left(\frac{C_b\omega}{F_s}\right) \tag{3}$$

$$m_{ij} = M_{ij}\left(\frac{C_b\omega^2}{F_s}\right) \tag{4}$$

The average bearing clearance C_b, running speed ω, and applied static load F_s are the measured during the dynamic tests.

Uncertainty Analysis

Two types of uncertainty arise while discussing dynamic data. The first type quantifies the repeatability of the bearing response during a dynamic excitation. The average dynamic-stiffness value at each excitation frequency has an associated uncertainty. Error bars on all dynamic-stiffness plots denote the repeatability at each excitation frequency.

The dynamic-stiffness uncertainty also includes the uncertainty from the baseline measurement. The baseline uncertainty is added to each dynamic-stiffness measurement using the root-sum-squares method. Standard procedures as outlined by Beckwith et al. [12] apply.

The dimensionless coefficients (c_{ij}, k_{ij}, and m_{ij}) contain uncertainty from both the dimensional coefficients (C_{ij}, K_{ij}, and M_{ij}) and the measured dynamic conditions F_s, C_b, and ω. These uncertainty values are combined using error propagation to find the uncertainty of the dimensionless stiffness, damping, and virtual-mass coefficients.

STATIC CHARACTERISTICS

Clearances

Figures 7 and 8 show the measured cold and hot clearance pad profiles for the original and modified bearing, respectively. Kluitenberg [13] provides a full statement of static characteristics including a comparison of eccentricity ratios, attitude angles, and measured pad temperatures. Space restrictions preclude their inclusion here.

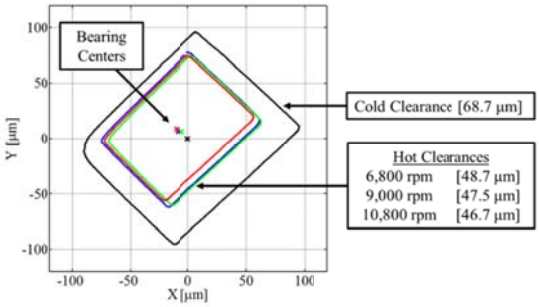

Figure 7. Original bearing measured pad profiles and bearing center

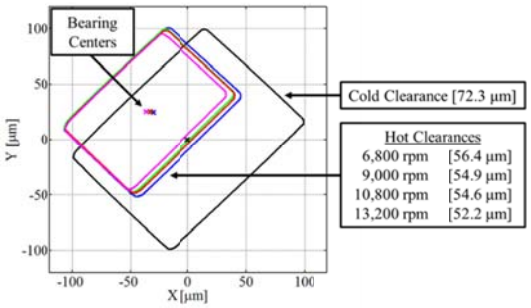

Figure 8. Modified bearing measured pad profiles and bearing center

Both bearings showed a decrease in bearing clearance with increasing running speed due to thermal expansion. Table 3 presents the average radial-bearing clearances estimated by fitting a circle to teach pad profile. Maximum pad temperature that is recorded just prior to taking the clearance measurement is also presented.

Table 3. Measured bearing cold and hot clearances and peak temperatures

Speed [RPM]	Original		Modified	
	C_b [µm]	T_{peak} [°C]	C_b [µm]	T_{peak} [°C]
0 (CC)	68.7	26.6	72.3	26.6
6,800 (HC)	48.7	84.2	56.4	93.7
9,000 (HC)	47.5	95.0	54.9	103.0
10,800 (HC)	46.7	102.1	54.6	109.2
13,200 (HC)	-	-	52.2	114.0

CC = *Cold Clearance* HC = *Hot Clearance*

DYNAMIC CHARACTERISTICS

This section compares the measured dynamic results for the bearing with and without JO ports. Comparisons are only presented where adding the ports makes an observable differences. Notably those include results for the direct damping and direct mass coefficients and do not include results for any cross-coupled coefficients.

Dynamic coefficients are plotted versus unit load. The error bars shown include the uncertainty from both the linear regression and the standard deviation of running speed, static load, and bearing clearance. For all measured dynamic results, circular data points connected by solid lines indicate the original bearing data taken from [1]. Square data points connected by dashed lines indicate the modified bearing data.

Dimensionless Direct Stiffness Coefficients

Figures 9 and 10 show k_{yy} and k_{xx}, respectively versus unit load for the original and modified bearing. Adding JO ports had no significant effect on the direct stiffness coefficients regardless of running speed and unit load. The change in dimensionless stiffness ranged from -9.1% to +0.6% for k_{yy}. The comparable changes for k_{xx} varied from -4.8% to 11.1%.

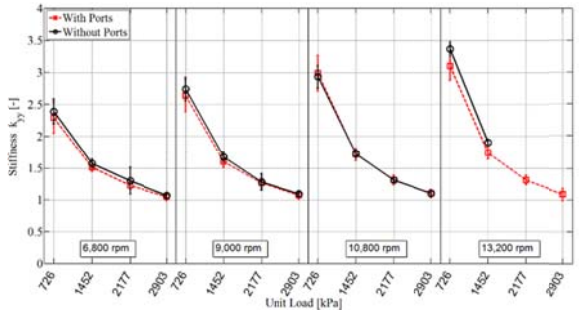

Figure 9. Direct stiffness coefficients k_{yy} (loaded direction)

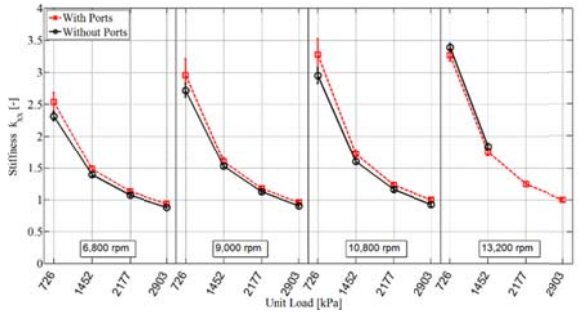

Figure 4. Direct stiffness coefficients k_{xx}

Dimensionless Direct Damping Coefficients

Figures 11 and 12 show c_{xx} and c_{yy}, respectively. Both decreased with increasing unit load and ω for both the original and the modified bearing. c_{xx} and c_{yy} decreased with the addition of JO ports. c_{yy} changed by -35% to -16%, with an average of -25.5%. c_{xx} changed between -16% and +1% with an average of -9.2%.

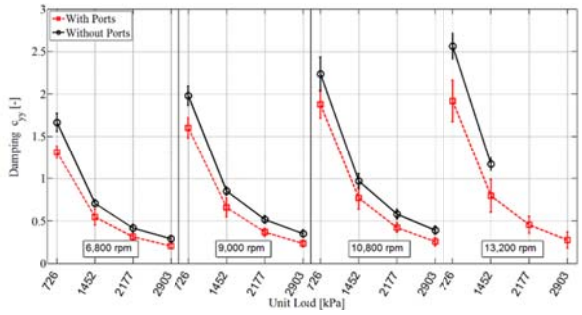

Figure 11. Direct damping coefficients c_{yy} (loaded direction)

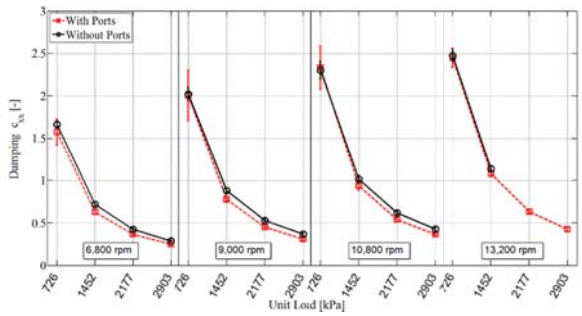

Figure12. Direct damping coefficients c_{xx}

Dimensionless Direct Virtual-Mass Coefficients

Figures 13 and 14 show m_{xx} and m_{yy}, respectively, for the original and modified bearings. The original bearing had negative direct virtual-mass coefficients. Adding JO ports caused an increase in m_{xx} and m_{yy} at all operating conditions; i.e., the modified bearing had negative virtual-mass terms that were smaller in magnitude and some small but positive coefficients.

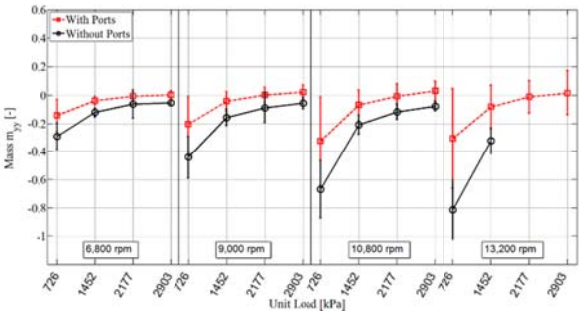

Figure13. Direct virtual-mass coefficients m_{yy}

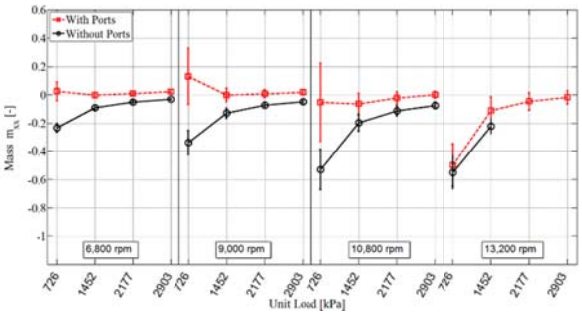

Figure14. Direct virtual-Mass coefficients m_{xx}

Recall that the virtual-mass coefficients are used to capture the frequency dependent dynamic stiffness, Re($\boldsymbol{H}_{ij}$) = K_{ij} - $m_{ij}\Omega^2$. Positive m_{ii} coefficients cause a "softening" effect or reduced bearing stiffness with increased Ω values. Negative m_{ij} coefficients cause a "stiffening" of the bearing at with increased Ω values. Figure 15 shows Re($\boldsymbol{H}_{ij}$) for both bearings at 6.8 krpm and 2.177 MPa (315.8 psi). Adding the JO ports decreases the dimensionless Re($\boldsymbol{h}_{xx}$) at 244 Hz (14,640 rpm) by 18%.

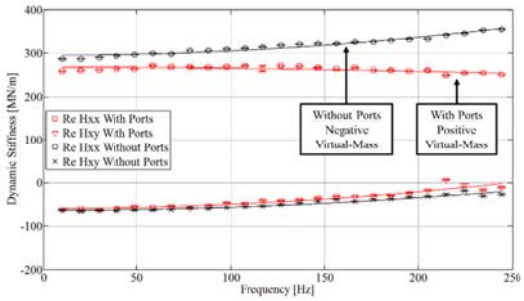

Figure15. Re($\boldsymbol{H}_{ij}$) with and without ports at 6,800 rpm and 2.177 MPa (315.8 psi)

RIGID-ROTOR-MODEL PREDICTIONS

The rigid-rotor model of Fig. 16 is used to address the question: *How will adding JO ports to a TPJ bearing affect the natural frequency and log decrement of a rotor-bearing system?* The rotor is supported by two identical bearings and has an added center mass of 303 kg that was chosen so that each bearing has a unit load of 0.725 MPa (105.3 psi). In addition, the models first damped natural frequency falls within the bearing-test speed range of 6.8 to 13.2 krpm. *Measured* dynamic coefficients from the original and modified bearings tests are used to model the bearings. Using a rigid-rotor model versus a flexible-rotor model exaggerates the impact of adding JO ports to a real machine; however, it gives a starting point in understanding the potential impact of JO ports.

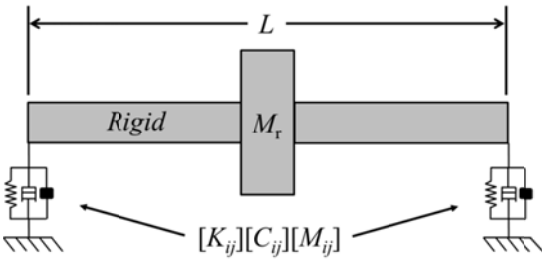

Figure16. Model of rigid rotor supported by TPJ bearings

The dynamic coefficients of the modified bearing were normalized to account for the change in clearance, via

$$\begin{Bmatrix} \tilde{K}_{ij} \\ \tilde{C}_{ij} \\ \tilde{M}_{ij} \end{Bmatrix}_{(Normalized)} = \left[\frac{C_{b,(Modified\ Bearing)}}{C_{b,(Original\ Bearing)}} \right] \begin{Bmatrix} K_{ij} \\ C_{ij} \\ M_{ij} \end{Bmatrix}_{(Modified\ Bearing)}$$

Figures 17 and 18 show, respectively, the predicted damped critical speed (ω = damped natural frequency) and its associated damping ratio, respectively, for the model with and without JO ports. When supported by the original bearing, the first damped critical speed is 12.4 krpm, and the damping ratio is 0.388. Adding JO ports reduces the damped critical speed to 10.5 krpm while increasing the damping ratio to 0.444. Recall from figures 11 and 12 that the modified bearing had lower direct damping values than the original bearing; hence, the drop in damping factor for the JO bearing is caused by the drop in critical speed that is in turn mainly caused by the increase in m_{yy} and m_{xx}. These trends would be expected for a flexible-rotor but with a reduced impact.

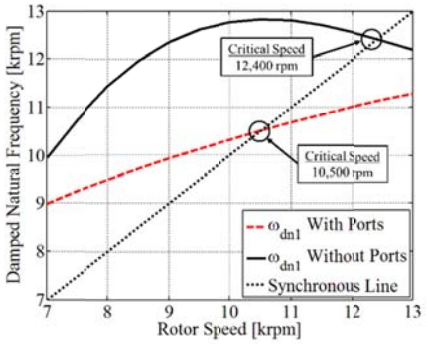

Figure17. Rotor damped natural frequency predictions with and without JO ports

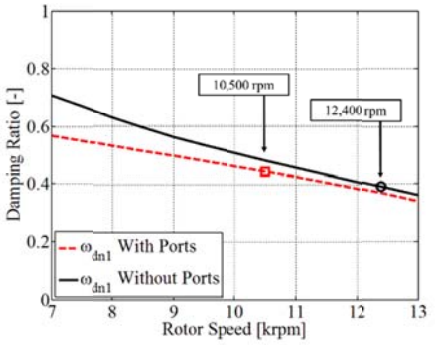

Figure18. Rotor damping ratio predictions with and without JO ports

DISCUSSION, AND CONCLUSION

Dynamic Coefficients

The static and dynamic characteristics of a TPJ bearing were measured before and after adding jacking-oil (JO) ports. The modified bearing was tested at four running speeds (6.8, 9.0, 10.8, and 13.2 krpm) and four unit loads (0.725, 1.452, 2.177, 2.903 MPa). Static and dynamic characteristics were separately measured for test condition; however, only dynamic data are presented here. Kluitenberg [13] provides a complete data set.

Adding JO ports produced significant decreases in c_{xx}, c_{yy} and increases in m_{xx}, m_{yy}. In the load direction, c_{yy} dropped by 35 to 16% with an average drop of 25.5%. In the orthogonal (x) direction, C_{xx} changed between -16% and +1%, with an average decrease of 9.2%.

The original bearing had negative m_{xx}, m_{yy} coefficients at all test conditions. The modified bearing showed an increase in m_{xx}, m_{yy} (smaller negative or slightly positive value).

Small changes were observed in the dimensionless coefficients k_{xx} (-4.8 to +11.1%), and k_{yy} (-9.1% to +0.6%). No significant changes were observed in any of the cross-coupled coefficients.

Predictions from an Idealized Rotordynamic Model

Predictions were made for a simple rigid-rotor bearing system to study how adding JO ports could affect the natural frequency and damping of a real machine. Measured dynamic coefficients were used for both TPJ bearings, and the added mass was selected to match the tested bearing unit load. For the original bearings, the first damped critical speed was 12.4 krpm with a damping ratio of 0.388. With JO ports, it dropped to 10.5 krpm with an increase in the damping ratio to 0.444. The observed changes in the predicted behavior were almost entirely caused by the observed changes in the virtual-mass coefficients.

The results presented suggest that implementing JO ports in a machine supported by tilting pad bearings will cause a drop in the observed 1st critical speed and an increase in its damping factor

ACKNOWLEDGEMENT

The work reported here was sponsored by the Turbomachinery Research Consortium (TRC) of the Texas A&M University System, Texas Engineering Experiment Station, Turbomachinery Laboratory.

NOMENCLATURE

A_i	Fourier Transform of stator accelerations [L/t^2]
C_b	Bearing clearance [L]
C_p	Pad clearance [L]
c_{ij}	Dimensionless damping coefficients [-]
C_{ij}	Direct and cross-coupled damping coefficients [F.t/L]
e_o	Static displacement [L]
$\boldsymbol{H_{ij}}$	Dynamic-stiffness [F/L]
$\boldsymbol{j}$	Imaginary unit, $\sqrt{-1}$ [-]
k_{ij}	Dimensionless stiffness coefficients [-]
K_{ij}	Direct and cross-coupled stiffness coefficients [F/L]
L	Pad axial length [L]
m_{ij}	Dimensionless virtual-mass coefficients [-]
M_{ij}	Direct and cross-coupled virtual-mass coefficients [M]
JO	Jacking-oil
x_o,y_o	Bearing center position [L]
x_r,y_r	Rotor center position [L]
γ	Attitude angle [Angle]
ε_0	Eccentricity ratio [-]
θ	Angular coordinate [Angle]
ω	Journal angular velocity [Angle/t]
Ω	Excitation frequency [1/t]

REFERENCES

[1] Tschoepe, D. and D. Childs, 2014, "Measurements versus Predictions for the Static and Dynamic Characteristics of a Four-Pad, Rocker-Pivot, Tilting-Pad Journal Bearing," *ASME J. for Gas*

Turbines and Power, 136 (1), May 2014, 136, pp. 052501-1-11

[2] Santos, I., and Russo, F., 1998, "Tilting-Pad Journal Bearings With Electronic Radial Oil Injection," *ASME Journal of Tribology*, **120(3)**, pp. 583-594.

[3] Varela, A., and Santos, I., 2015, "Dynamic Coefficients of a Tilting Pad With Active Lubrication: Comparison Between Theoretical an Experimental Results," *ASME Journal of Tribology*, **137(3)**, Paper 031704.

[4] Hattenbach, T., and Sandberg, M., 2009, "Influence of Jacking Oil Supply Configuration on Shaft Vibration of a Super-Synchronous Motor," PowerPoint, *Proceedings of 38th Texas A&M Turbo Symposium*. Case Study 06.

[5] Hagemann, T., Sebastian, K., and Schwarze, H., 2013, "Measurement and Prediction of the Static Operating Conditions of a Large Turbine Tilting-Pad Bearing Under High Circumferential Speeds and Heavy Loads," *Proceedings of ASME Turbo Expo 2013*, GT2013-95004, June 3-7, 2013, San Antonio, Texas

[6] Ressing, H., Köster, P., Ziegler, K.,Conlon, M., Dadouche, A., Evans, D., and D. Turton, (2013), "Influence of Jacking Oil Grooves in Two-Lobe Bearings on Bearing Performance," Proceedings, case study 42nd Turbomachinery Symposium, Turbomachinery Laboratory, Texas A&M University

[7] Glienicke, J., 1967, "Experimental Investigation of the Stiffness and Damping Coefficients of Turbine Bearings and their Application to Instability Predictions," *Proceedings of the International Mech. E.*, **181** (3B), pp. 116-129.

[8] Kulhanek, C., 2010, "Dynamic and Static Characteristics of a Rocker-Pivot, Tilting-Pad Bearing with 50% and 60% Offsets," M.S. thesis, Mechanical Engineering, Texas A&M University, College Station, TX.

[9] Gaines, J., 2015, "Examining the Impact of Pad Flexibility on the Rotordynamic Coefficients of Rocker-Pivot-Pad Tilting-Pad Journal Bearings," M.S. thesis, Mechanical Engineering, Texas A&M University, College Station, TX.

[10] Coghlan, D., and D. Childs (2015), "Characteristics of a Spherical Seat TPJB With Four Methods of Directed Lubrication – Part 2: Rotordynamic Performance", Paper number GT2015-42336, Proceedings of ASME Turbo Expo 2015, 15-19 June 2015, Montréal, Canada (accepted for Journal publication)

[11] Rouvas, L., and Childs, D., 1993, "A Parameter Identification Method for the Rotordynamic Coefficients of a High Reynolds Number Hydrostatic Bearing," *ASME Transactions*, **115**, pp. 264-270.

[12] Beckwith, T., Marangoni, R., and Leinhard, J., 1995, "*Mechanical Measurements: Fifth Edition*," Addison-Wesley Publishing Company Inc., Reading, Massachusetts, pp. 857-859.

[13] Kluitenberg, M., 2015, "Experimentally Determine The Impact Of Jacking Oil Pockets On The Rotordynamic Characteristics Of A Four-Pad, LBP, Tilting-Pad Journal Bearing, M.S. Mechanical Engineering Thesis, May 2015, Texas A&M University